한국해양환경공학회지
Journal of the Korean Society
for Marine Environmental Engineering
Vol. 13, No. 2. pp. 91-98, May 2010

OWC 파력발전장치의 공기실 성능예측에 대한 수치적인 연구

김길원[1] · 현범수[1,†] · 류 진[2] · 홍기용[3]
[1]한국해양대학교 조선해양시스템공학부
[2]중국해양대학교 산동성중점해양공학실험실
[3]한국해양연구원 해양시스템안전연구소

Numerical Prediction of Chamber Performance for OWC Wave Energy Converter

Ji-yuan Jin[1], Beom-soo Hyun[1,†], Zhen Liu[2] and Keyyong Hong[3]
[1]College of Ocean Science and Technology, Korea Maritime University, Busan, Korea
[2]Shandong Province Key Laboratory of Ocean Engineering, Ocean University of China, Qingdao, Chian
[3]Maritime and Ocean Engineering Research Institute, KORDI, Daejeon, Korea

요 약

진동수주형 파력발전장치에서 공기실 내의 수면 변화와 덕트 내 유량의 왕복유동은 시스템의 작동 성능을 결정짓는 매우 중요한 요소이다. 공기실 내의 수면 변화를 고찰하기 위하여 상용 CFD 코드인 Fluent 6.2를 이용하여 구현한 수치조파수조를 사용하였다. 수치조파수조의 지배방정식은 연속방정식과 Reynolds 평균 N-S 방정식이고 자유수면은 Two-phase VOF 기법을 이용하여 추적하였다. 공기실 내의 수면 변화와 공기실 윗부분에 설치된 덕트 내의 왕복유량을 계산하여 고찰하였고, 계산의 정확도를 검증하기 위하여 실험결과와 비교 분석을 수행하였다. 또한 동일한 입사파 조건에서 공기실 - 덕트 시스템의 노즐 비율이 시스템이 미치는 영향을 고찰하여 분석을 하였다.

Abstract – The water elevation inside the air chamber and bi-directional air flow in the duct of Oscillating Water Column wave energy converter is one of the most important factors to evaluate the operating performance. The numerical wave tank based on the commercial software Fluent 6.2 in the present paper is employed to generate the incident waves. The numerical wave tank consists of the continuity equations, the Reynolds-averaged Navier-Stokes equations and the two-phase VOF function. The oscillating amplitude of water column in the chamber and bi-directional air flow in the duct installed on the top of the chamber are calculated, and compared with experimental data to verify the validation of the present NWT. The nozzle effects of the chamber-duct system on the relative amplitudes of the inner free water surface and air flow rate in the duct are investigated.

Keyword: Wave energy converter(파력발전변환장치), Oscillating water column(진동수주), Operating performance(작동성능), Numerical wave tank(수치조파수조), Nozzle ratio(노즐 비율)

1. INTRODUCTION

Wave energy is one of the most promising forms of ocean renewable sources because of its high energy density. The oscillating water column (OWC) device has been widely employed in the wave energy conversion. It comprises a partially submerged air chamber with an underwater opening in the front skirt, and the water column exposes to the incident wave field through the opening. Waves can force the water column in the chamber to oscillate in the same manner as a simple piston, which will produce the bi-directional air flow through the air turbine in the duct. Capable of operating in the reversing flow conditions, the Wells turbine or the impulse turbine linked to the electric generator in the air duct, is generally

†Corresponding author: bshyun@hhu.ac.kr

used to convert the air static and dynamic pressure into the mechanical energy. The converting efficiency is related to the incident wave conditions and shape parameters of the chamber-duct system.

A number of efforts have been made to study the performance of OWC air chamber. Hong *et al*. [2007] performed an experiment concentrating on the effects of several shape parameters of OWC chamber in wave energy absorbing capability. Lee *et al*. [1996] first utilized low order 3D boundary element methods to predict the response of an isolated OWC accounting for the appropriate interior free surface boundary condition. Hong *et al*. [2004] calculated the motions and time-mean horizontal drift forces of floating backward-bent duct buoy wave energy absorbers in regular waves taking account of the oscillating surface pressure due to the pressure drop in the air chamber above the oscillating water column within the scope of the linear wave theory. Josset and Clement [2007] applied the low order boundary element method for efficient hydrodynamic modeling of generic bottom mounted OWC power plants to estimate the annual performance of the wave energy plant on Pico Island.

It can be seen that most of former numerical simulations just focus on the oscillating amplitude of the inner water column, which is employed to show the wave energy absorbing performance of the air chamber totally open without covers. While Hong *et al*. [2004] has studied the effects of ratio between the sectional areas of chamber and duct, the air damping coefficient they adopted still needs to be determined a priori. It has been pointed out that the wave motion in the opening chamber is quite different from that for the chamber with the cover by Hong *et al*. [2007]. However, the oscillating amplitude of the water column in the chamber with an air duct should be investigated to show the performance of the chamber-duct system. Furthermore, the air flow velocities in the duct, which demonstrates the wave energy converting capability more accurately, should be studied. It is also necessary to establish a numerical method to simulate the air flow motion in the duct and water-air interaction at the free surface directly.

In the present paper, a numerical wave tank using two-phase VOF model based on the commercial CFD code Fluent V 6.2.16 is utilized to simulate the generation and propagation of incident regular waves, oscillating water column inside the chamber and air flow motion in the duct, which are validated by the corresponding experimental data. The nozzle area ratios of the chamber-duct system are then calculated to illustrate its effects on the wave energy absorbing capability.

2. NUMERICAL WAVE TANK

The incident waves are 2D and 3D regular waves, which are generated by the piston motion of the wave making plate at one end of the flume. The schematic of numerical wave tank and the coordinate system are shown in Fig. 1, where is the still water depth; B and L are the calculating width and length of the numerical tank.

2.1 Governing Equations and Numerical Solutions

In the present study, the numerical waves are generated by the commercial computational fluid dynamics software Fluent 6.2, which is employed to solve the incompressible fluid flow based on the 2D and 3D Reynolds-averaged Navier-Stokes equations. The standard k-ε model, which is widely used in engineering application, is employed to describe the turbulence phenomenon in the water and air dynamic motions, such as wave breaking and intense water-air interaction. The tracking of the interface between the air and water phases is accomplished by the Volume of Fluid (VOF) method (Hirt and Nichols [1981]).

Because of the regular waves employed in this paper, the piston wave maker is applied in the wave generating and the Sommerfeld radiation boundary condition is utilized at the opening conditions (Sommerfeld A. [1949]). The wave absorption can be performed by controlling the motion of the opening boundary within the velocities opposite to the water particles adjacent to the opening boundary on the x-direction.

The NITA (None-Iterative Time Advancement) - PISO (Pressure Implicit with Splitting of Operators) algorithm compatible with VOF model, which requires only one global iteration per time step and reduces solution time significantly, is employed for the pressure-velocity coupling. The geometric reconstruction scheme and body force-weighted scheme are utilized for the VOF model and pressure interpolation respectively.

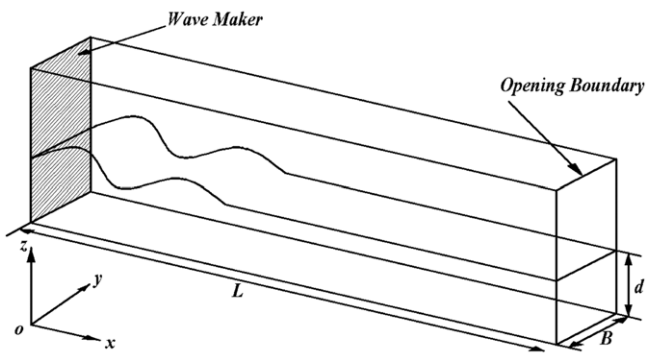

Fig. 1. Schematic of the numerical wave tank.

The motion of the wave generating and absorbing boundaries can be achieved by defining UDF (User-Defined Function) programs. Fluent also provides the layering remeshing method in dynamic mesh model to govern the grid reconstruction adjacent to the moving boundaries. The geometries and meshes are created by the grid generation software Gambit V 2.2, and the grids at the fluid interface have been refined to predict the free surface accurately. The symmetric boundary conditions provided by Fluent software are applied for the wave making and absorbing boundaries. The bottom and chamber structure is set as the wall using no-slip conditions. The pressure outlet is taken account for the upper boundaries of the computational domain adjacent to the air phase.

2.2 Validation Results

A validation computation of 2D and 3D regular waves was carried out to show the capability of the present numerical model. The tank length is 200 m, the water depth is 16m and the flume width in 3D tank is 13.72 m, respectively. The maximum displacement of wave maker plate S_0 is 0.8 m, and the incident wave period T is 3.5s. The calculating time step is set as 0.005s. The grid independency and effects of time step have been tested, and the computational results indicate that the numerical accuracy will be ensured when the grid size is less than $L/20$ and time step is less than $T/50$, where L denotes the wave length. In the present simulation, the grid sizes were adjusted according to the wave length. In the present study, the grid size in the x-direction Δx was set around $L/50$, and Δy in the y-direction was around h/20. The temporal time step was set to $T/100$ according to the incident wave period.

The grid numbers of 2D and 3D NWT are about 1.8×10^4 and 1.2×10^5, respectively. The computing time for one case in 2D and 3D NWT are around 2hrs and 6hrs. Although the computing time is much longer than that of the traditional linear flow models, it should be noted that the longer calculating time is the price of obtaining the precise prediction of the air flow motion, which can not be easily achieved in the potential wave models and is critically important in the performance analysis of the air chamber of the oscillating water column of wave energy device.

Example of the instantaneous 3D wave profile is given in Fig. 2, showing that the 3D equable waves can be generated and propagate in the flume. The numerical results for the time series of wave elevation at the position of x=30 m in the numerical wave flume, and the comparison with the corresponding analytical solutions are shown in Fig. 3. It can be seen that the

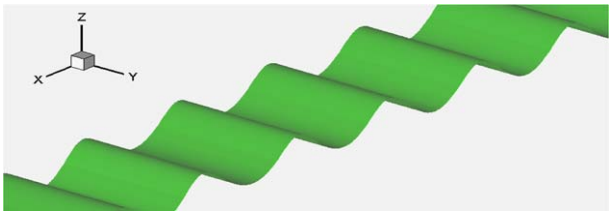

Fig. 2. Example of 3D instantaneous wave profile.

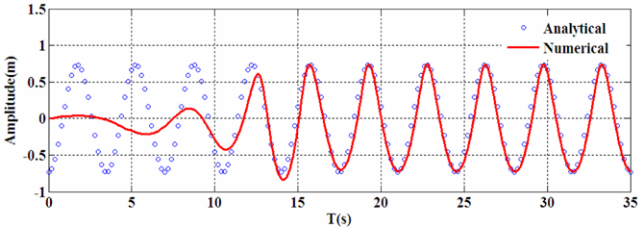

Fig. 3. Time series of wave elevation at the position of x=30 m.

numerical predictions agree well with the analytical solutions after the initial transient effect has diminished.

In general, the present NWT can generate both 2D and 3D regular waves within desired wave periods and heights. The opening boundary has good capability of absorbing the incident waves so that the numerical wave simulation can be run for a long time.

3. NUMERICAL ANALYSIS of OWC AIR CHAMBER

3.1 Applications of Two-phase VOF NWT

The schematic of the OWC air chamber with an cylinder duct installed at the center of the top cover is shown in Fig. 4, where l_f denotes the chamber width, d_s the draft of the chamber skirt, l_s the thickness of the chamber skirt, l_d the diameter of the cylinder duct, h_d the length of the duct. The still water depth is

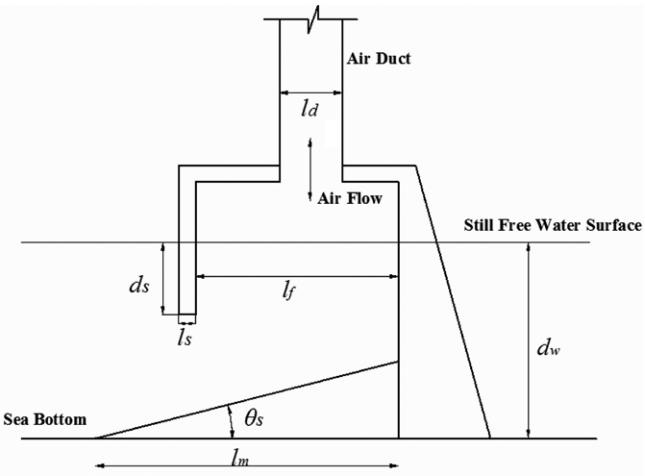

Fig. 4. Schematic of OWC chamber-duct system.

Table 1. Calculating Cases with various test conditions

Case	l_f (m)	l_s (m)	d_s (m)	l_d (m)	A	h_d (m)	a_0 (m)	NWT
1	1.5	1.0	2.5	1.5	1.0	0.0	0.38	2D
2	6.0	1.0	3.5	6.0	1.0	0.0	0.5	2D
3	6.0	1.0	2.5	2.5	2.4	13.7	0.5	2D, 3D
4	6.0	1.0	2.5	1.5	46.6	13.7	0.5	2D, 3D
5	6.0	1.0	3.5	1.5	46.6	13.7	0.5	2D, 3D

d_w=16 m. The slope angle of bottom θ_s and the base length of the slope l_m are fixed as 26° and 23 m, respectively.

Five cases with various test conditions are summarized in Table 1, where a_0 is the incident wave amplitude. The contents in last column represents which type of the numerical wave tank will be applied in this case. In the first two cases, l_d equals to l_f, and h_d is zero, which means the top of the chamber is totally open with any covers. For case 3~5, the top of the chamber is partially open along the whole length. The dimensionless nozzle area ratio A employed in the investigation is defined as:

$$A = A_C/A_D \tag{1}$$

where A_C is the sectional area of the chamber, and A_D is the sectional area of the duct.

The incident waves whose period varies from 3.5s to 8s are employed for each case. In the numerical simulation, the OWC chamber is set at the end of the wave tank, which is opposite to the wave maker plate. The wave amplitude in the chamber denoted by a is recorded in the center of the chamber for all the cases. The air flow rates in the duct at the position 8 m higher from the top of the chamber are measured automatically for Case 3~5. The corresponding experiments for these cases were carried out in the laboratory wave flume of MOERI, Korea. The model ratio is 1:23, the acryl chamber model is fixed at the opposite to the wave maker. The wave elevation data were measured by the wave gauges in the chamber.

The dimensionless relative wave amplitude a/a_0 is used to illustrate the water column elevation in the chamber. Time histories of a/a_0 for case 1 and 2 within the incident wave period T=6.0s calculated in 2D NWT are given in Fig. 5. It can be seen that the oscillating periods of the inner water column are almost equal to the incident wave period. For the small chamber width in Case 1, the oscillating behavior of water column is sinusoidal, which is similar with the incident regular wave. When the chamber width increases in Case 2, the free surface elevation is more complicated because of the standing wave formation inside the chamber, which also has been observed in the experiments.

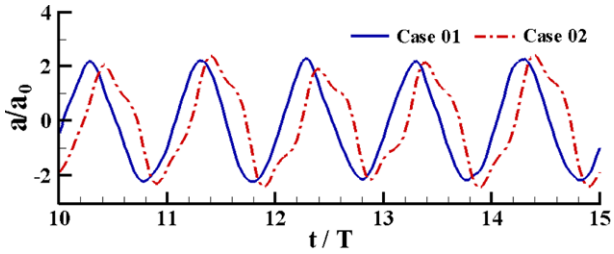

Fig. 5. Water column elevation in the chamber (T=6.0s).

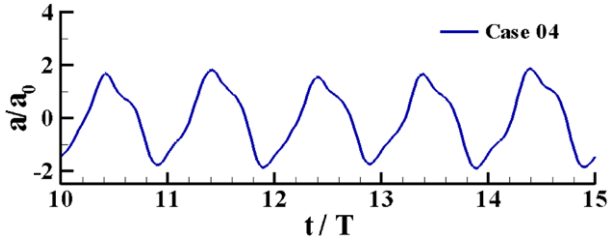

Fig. 6. Water column elevation in the chamber (T=6.0s).

As shown in Fig. 6, the free surface elevation in the chamber with a cylinder duct shows quasi-sinusoidal oscillation. Comparing with the chamber without any cover in Case 2, the relative amplitude reduces because of higher air pressure in the chamber induced by the duct system. Similar with the numerical results, it can also be found that the positive values of the oscillating amplitude show a tendency somewhat higher than the negative values in the corresponding experiments. The corresponding time history of the relative pressure in the chamber for Case 4 is presented in Fig. 7. The pressure shows a phase difference with the water column oscillating in the chamber. It can be explained that the pressure variations are induced by the free surface elevation, which is also affected by the air pressure in the chamber, incident wave length and the viscosity. The pressure is monitored at several points in one section inside the chamber and the mean values are plotted in Fig. 7. The irregular variation of the pressure field is likely to be caused by rather nonuniform distribution of pressure field at different monitoring points. The oscillating behavior of the air velocity in the duct given in Fig. 8 is more stable mainly due to the contraction effect of nozzle. The periods of free surface elevation, the air pressure and the air flow velocity variations are

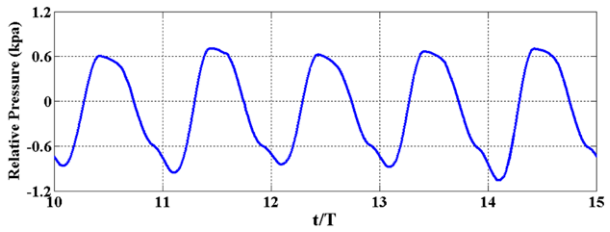

Fig. 7. Time history of relative pressure in the chamber (case 4, T=6.0s).

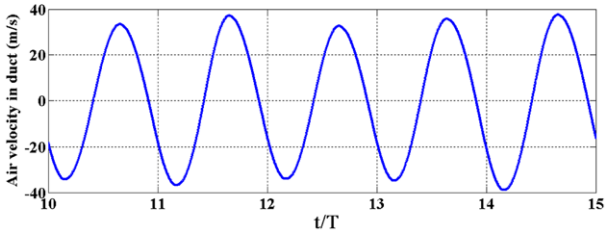

Fig. 8. Time history of air velocity in the duct (case 4, T=6.0s)

same as the incident wave period.

The computational oscillating amplitudes of the water column in the chamber with respect to incident wave periods for Case 1~2 are calculated. The relative wave amplitude variation against the dimensionless number, wave length ratio is shown in Fig. 9 (a). is the incident wave length, which varies within the incident wave periods. The resonant wave length ratios are obvious where the peak values of the relative wave amplitudes occur. It will converge to around 2 when the wave length ratio increases, where the standing waves are observed to be formed in front of the chamber. The numerical predictions agree well with the experimental data, except that the distribution shows a little shift to the larger incident wave length.

Fig. 9(b) displays the comparison between calculated and laboratory results of relative amplitude distribution for Case 2. It can be seen that the peak are not identical when the air chamber has a larger width. The relative amplitudes also converge to about 2 when the wave length ratios are larger than 8. The good agreement between the numerical and experimental results indicates that the present numerical model can predict the variation of the distribution of the chamber without any covers. Some discrepancies in Fig. 9 is likely induced by the effect of chamber length, which is very sensitive to the incident wave length. For the smaller chamber length, the resonant period will be generated and it can be found significantly in the case with larger length.

In the study of the chamber with an air duct, the system can be simplified to 2D dimension directly for Case 3 and the area ratios for the duct diameters are considered in Case 4 and 5, when the 2D NWT are utilized.

For the 3D calculation, the chamber length is 13.72 m. The numerical and experimental results of relative wave amplitudes when the monitor point is at the center of the chamber for Case 3~5 are displayed in Fig. 10. Generally, 2D and 3D simulations show little difference on the predicting capability of the free surface elevations at the center of the chamber. For case 3, the numerical result shows a little smaller value at the short period domain, and, for case 5, it is smaller at the long period domain. These discrepancies may be due to the interactions among chamber dimensions and wave condition, and also some inaccuracies in the numerical model. Further investigation will be made in near future. Furthermore, the calculated results agree well with the experimental data, except the 3D flume is superior to the 2D model in the larger wave length ratio's domain for Case 5. The results also show that all the relative amplitudes converge to around 2 when the wave length ratios increase to infinity, and it indicates that the

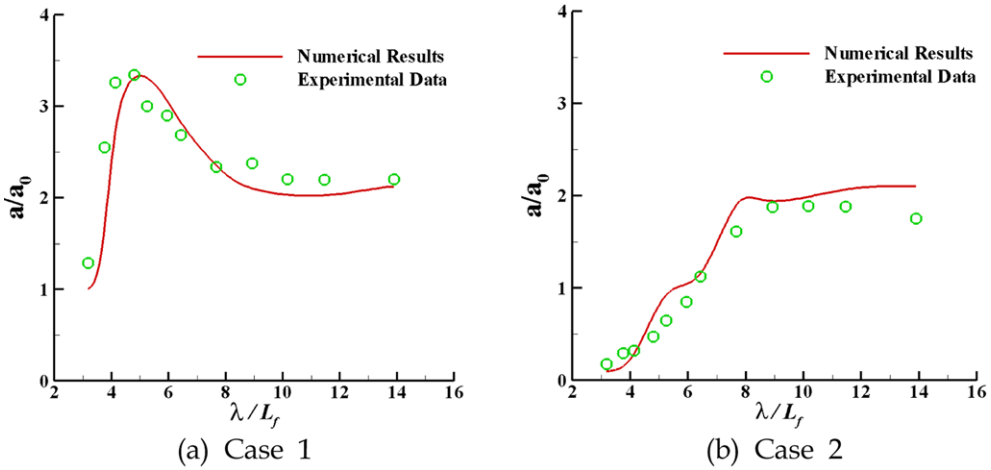

Fig. 9. Relative wave amplitude distribution with the wave length ratio variation.

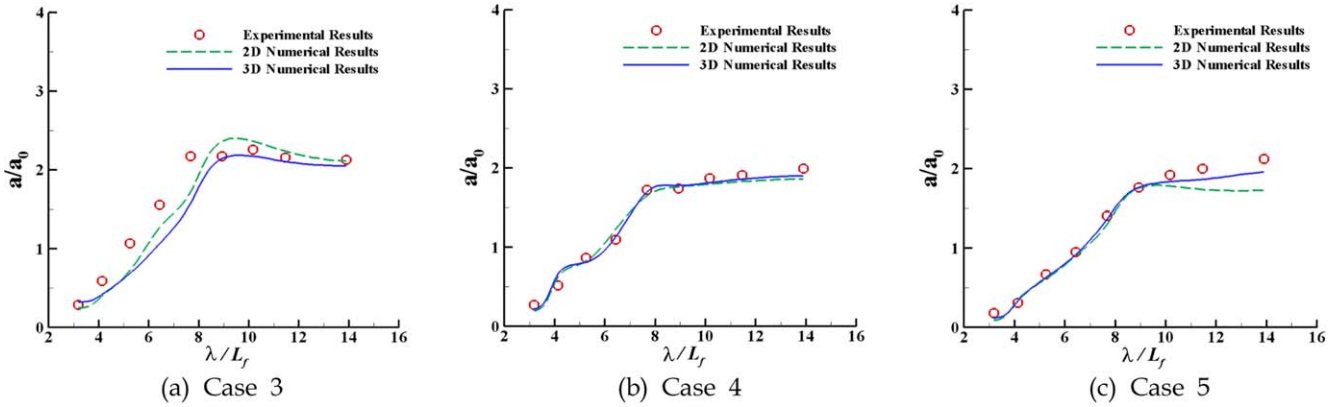

Fig. 10. Comparison of relative wave amplitude distributions with the wave length ratio variation (Monitor point at the center of the chamber).

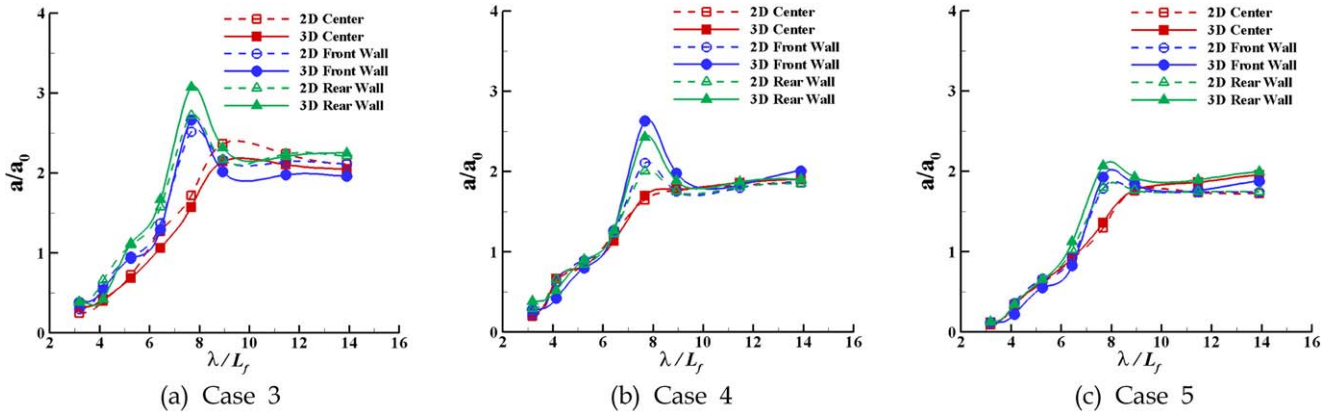

Fig. 11. Comparison of relative wave amplitude distributions with the wave length ratio variation at different monitor points.

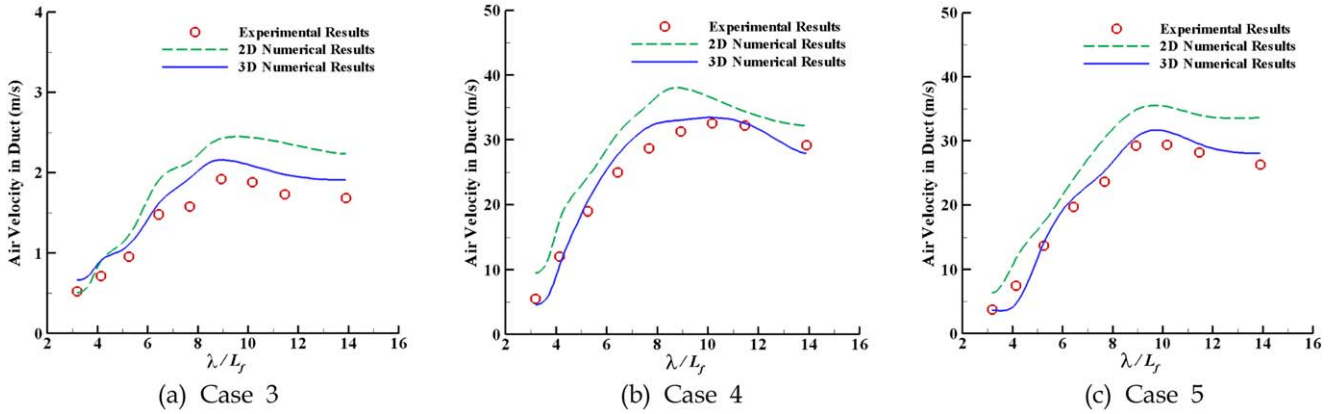

Fig. 12. Comparison of positive amplitude distributions of the air flow velocity in the duct with the incident wave period variation.

chambers with large scales and more air volumes inside have wide bands for the effective wave energy converting wave length ratios.

The comparison between the 2D and 3D numerical results of the relative wave amplitudes at different monitor points are shown in Fig. 11. The resonant wave length ratio is around 8 near the front and rear walls where the maximum relative wave amplitudes occur both in 2D and 3D NWTs. The peak values predicted by the 3D NWT are higher than that from 2D flume in Case 3~5. Except at the resonant wave length ratios, the difference of the relative amplitudes at various monitor points of the chamber in the 2D simulation is minor especially for the larger wave length ratios. On the other hand, the accurate prediction of the oscillating amplitude distributions in the chamber demonstrates that the present 3D model can predict the complicated free surface motion with large amplitudes such as

sloshing, which also has been observed in the corresponding experiments.

The positive amplitude distributions of the air flow velocity in the duct with respect to the wave length ratios are shown in Fig. 12. It can be seen that most of the numerical predicted values are larger than the corresponding experimental data. However, the results obtained by the 2D model are obviously overestimated, and the 3D calculated air flow velocities satisfactorily agree with the experimental results. The overestimations in the 2D calculation are induced by the simplification of the chamber-duct system. It cannot predict accurately the complicated free water surface elevation including the standing waves formation and sloshing motion of the water column as seen in Fig. 11.

The above comparisons illustrate that both 2D and 3D numerical models are capable of simulating the water column oscillation inside the chamber. Comparing with the overestimation of 2D NWT, the 3D model has the good performance on the prediction of the air flow motion, which indicates that it also can accurately calculate the air pressure variation in the chamber-duct system.

3.2 Effects of Nozzle Area Ratios

The reversing air flows in the duct are generated from the variation of the air pressure in the chamber, which has the dynamic interaction with the water column in the chamber. Different air duct sizes induce different air pressure acting on the free water surface in the chamber. The changes of the oscillating amplitudes of the water column then counteract the air pressure, which will induce the different air flow rates in the duct.

In the present study, the chamber length and width are set as 13.72 m and 8.0 m, respectively. The cylinder duct diameter varies from 1.0 m to 3.0 m, and the chamber totally open without any cover (A=1) is also utilized to illustrate the effects the nozzle area ratio. A typical wave length ratio $\lambda/l_f = 6.7$ is selected for the investigation because the relative wave amplitudes are observed to converge at its corresponding incident wave period T=6.0s.

Fig. 13(a) presents the effects of nozzle area ratio on the area-averaged relative wave amplitudes a/a_0 inside the chamber. When the nozzle area ratio increases according to the increase of the sectional area of chamber, the relative wave amplitude reduces significantly. In addition, the relative wave amplitude decreases when the nozzle area ratio increases because the larger air pressure which will confine the free surface elevation in the chamber.

As shown in Fig. 13(b), the positive amplitudes of air flow rates in the duct also decreases when the nozzle area ratio increases due to the corresponding free surface oscillating amplitudes. It should be noted that the variation of the air flow rates is minor when the nozzle ratio is less than 40. For the smaller duct diameters, the higher air pressure in the chamber causes unstable wave elevation and more frequent and complex air water interaction with energy loss which cannot contribute to the air flow in the duct, so the variation of the air flow rates is more evident with respect to the nozzle ratios. Furthermore, the nozzle area ratios have more effects on the air flow rates when it is larger than 40.

Comparatively, the air flow velocity shows almost linear varying tendency in Fig. 13(c). The investigation of the air flow velocity in the duct is also important for the OWC wave energy power plants.

During the design of the turbine with the desired power output, it is hard to get a large duct diameter with higher velocities contemporarily as shown in Fig. 13(a) and (b). Therefore, it is necessary to consider the duct size, the air flow rate and

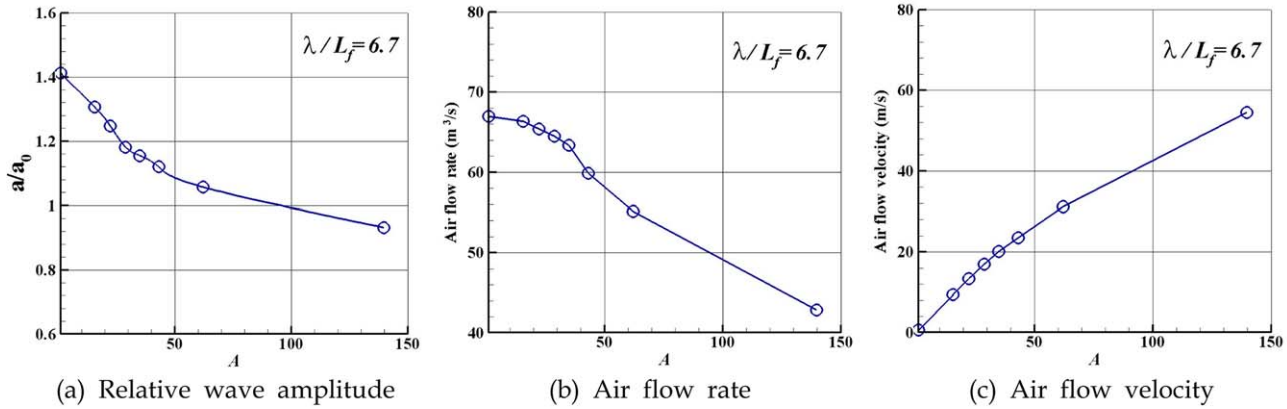

Fig. 13. Effects of nozzle area ratios on the wave energy absorption.

the velocity coherently for the optimal design of the turbine.

4. CONCLUSIONS

A numerical wave tank using two-phase VOF model was established to generate the propagating waves. The standard turbulence model, NITA-PISO algorithm and dynamic mesh method were also employed. Both 2D and 3D regular waves were validated by the analytical solutions.

The OWC air chamber was fixed at the end of the NWT. The present numerical model could predict the oscillation of the free water surface, the variation of the air pressure in the chamber and air flow motion in the duct. It was found that the oscillating amplitudes of the wave elevation in the chamber obtained from the 2D NWT coincided well with the experimental data. The overestimation of the air flow in the duct illustrated its limits in the corresponding analysis because of its simplification of the chamber-duct system during the calculation.

However, the 3D NWT showed its superiority to the 2D NWT. The good agreements with the laboratorial results demonstrated its capability on the prediction of the free surface elevation of the water, the variation of the air pressure, the dynamic motion of the air flow and their relative interaction. It was concluded in general that the 3D numerical wave tank is a reasonably good prediction tool in the analysis of the OWC air chamber especially in the investigation of chamber-duct system.

Finally in the numerical simulation, the nozzle area ratio had nearly identical effects on the relative amplitude in the chamber, the air flow rate and velocity in the duct. It was found to be necessary to consider the effects of the air duct size, the air flow rates and the corresponding velocities coherently for the optimal design of the air turbine and the OWC power plant.

ACKNOWLEDGEMENTS

This research is financially supported by Korea Ocean Research & Development Institute and Korea Ministry of Land, Transport & Maritime Affairs (Development of Wave Energy Utilization System). All the support is gratefully acknowledged.

REFERENCES

[1] Hirt, C.W. and Nichols, B.D., 1981, “Volume of Fluid (VOF) Method for the Dynamics of Free Boundaries”, J Comp Phys, Vol 39, pp 201-225.

[2] Hong, D.C., Hong, S.Y. and Hong, S.W., 2004, “Numerical Study on the Reverse Drift Force of Floating BBDB Wave Energy Absorbers”, Ocean Engineering, Vol 31, pp 1257-1294.

[3] Hong, K.Y., Shin, S.H., Hong, D.C., Choi, H.S. and Hong, S.W., 2007, “Effects of Shape Parameters of OWC Chamber in Wave Energy Absorption”, Proc 17th Int Offshore and Polar Eng Conf, Lisbon, Portugal, ISOPE, Vol 1, pp 428-433.

[4] Lee, C.H., Newman, J.N. and Nielsen, F.G., 1996, “Wave Interaction with an Oscillating Water Column”, Proc 6th Int Offshore and Polar Eng Conf, Los Angeles, USA, ISOPE, Vol 1, pp 82-90.

[5] Josset, C. and Clement, A.H., 2007, “A Time-domain Numerical Simulator for Oscillating Water Column Wave Power Plants”, Renewable Energy, Vol 32, pp 1379-1402.

[6] Sommerfeld, A., 1949, “Partial Differential Equation in Physics”, Academic Press, New York.

2010년 3월 10일 원고접수
2010년 4월 6일 심사완료
2010년 4월 7일 수정본 채택